Application of system identification technique in efficient model test correlations for a floating power system

Hao Wang*, Abhilash Somayajula, Jeffrey Falzarano

Texas A&M University, College Station, Texas, USA

ABSTRACT

Both the time domain simulations based on potential flow theory and wave tank model tests are used to evaluate the motion responses of a wave energy device. In this work, system identification is applied to obtain the frequency dependent transfer functions (between motions and excitations) from a series of model test runs of a wave energy platform exposed to irregular (random) waves. This is the first application of Reverse-Multiple Input Single Output (R-MISO) to a realistically (catenary) moored system (typical characteristics of wave energy devices) comparing physical model tests with our in-house time domain simulation program with addition of a mooring model. Based on the comparisons between the transfer functions from the time domain simulations and those from the model tests, reasonable frequency dependent dampings have been directly pulled out from the test cases under random sea states. System identification derived corrections to the linear or quadratic damping in pitch significantly improved the accuracy of motion responses. In this sense, this methodology can be a powerful tool in assisting the accurate simulation and design of wave energy devices under random sea states.

Keywords: System identification, Reverse-Multiple input single output, Pitch damping, Reverse-Single input single output, Coherence function, Floating power system

1. Introduction

Ocean wave energy is a promising renewable energy resource that is distributed extensively in oceans and coastal areas worldwide. Wave energy converters (WEC) are structures designed to convert wave energy to electricity [1]. Numerous researchers and engineers have been making efforts to innovate, develop and optimize WECs. Typical WEC includes oscillating water column [2], attenuator, point absorbers, oscillating wave surge converter, submerged pressure differential devices, etc. [3]. Besides the electricity generating elements, the wave energy system also consists of supporting elements (e.g. grid connection and control). Designing these structures requires accurate predictions of their motion responses under a wide range of sea states (especially the incident waves).

In this study, simulations are performed using the in-house time domain simulation program, SIMDYN [4-6]. SIMDYN was originally developed to simulate the motions of ships [7,8]. After coupling with the open source Mooring Analysis Program (MAP++) [9] and making other modifications (e.g. incorporating the slowly varying wave drift forces [10]), the program is used to simulate the motions of the wave energy devices in Marine Dynamics Laboratory (MDL) at Texas A&M University. The modified SIMDYN takes frequency domain results such as added mass, radiation damping and excitation forces from the in-house frequency domain hydrodynamics analysis program MDL-HYDROD [11, 12] (similar to WAMIT or AQWA LINE).

Corresponding author, PhD candidate.
Email address: haowang8901@gmail.com (H. Wang), s.abhilash89@gmail.com (A. Somayajula), jfalzarano@civil.tamu.edu (J. Falzarano)

Model test are considered as the "gold standard" for examining WEC performances (e.g. [13]). The wave time series measured in the model test can be input to SIMDYN to compare SIMDYN simulated responses with those from the model tests. In this research, the model tests data are open source and accessible from Beaufort Research (HMRC) based in Cork, Ireland [14]. At the Galway Bay wave energy test site, a floating power system (FPS) was designed to supply power, collect data, as well as connect to the local grid (a similar system has been discussed in [15]). This FPS has been chosen as the benchmark model (like in [16]) to verify the simulation program SIMDYN (using the hydrodynamic forces from the frequency domain program MDL-HYDROD). The FPS has been tested in both regular (single frequency) and irregular (random) wave cases that were determined based on the sea state records of Galway Bay.

Viscous damping plays an important role in simulating the motion responses accurately and that is where the corrections based on the model test correlations become critical. Correcting the results for viscous damping can be achieved through empirical methods [17] or through free decay tests [16]. However, for the FPS, empirical equations for typical geometry may not be applicable. Unfortunately, the free decay model test result for the FPS was also not available.

Alternatively, the actual damping of the model could be evaluated using system identification [18]. Popular system identification techniques include Restoring Force Surface (RFS) [19, 20], Nonlinear Auto-Regressive Moving Average with eXogenous inputs (NARMAX) [21, 22], Hilbert transform [22, 23] and Reverse-Multiple Input Single Output (R-MISO) [23-

27]. Somayajula and Falzarano [18] have reviewed and discussed the advantages and limitations of these methods when applied to marine structures.

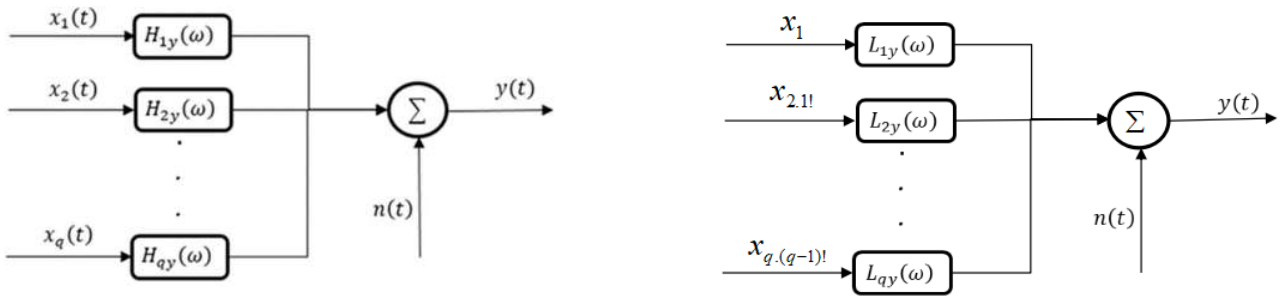

(a) q original inputs $x_i(t)$ and one output $y(t)$.

(b) q conditioned inputs $x_{i.(i-1)!}(t)$ and one output $y(t)$.

Fig. 1 MISO model with unconditioned inputs and conditioned inputs

The Marine Dynamics Laboratory (MDL) [28-31] has developed an analysis program using the R-MISO technique. From system identification, we are able to obtain the actual (pitch) effective damping from the FPS model tests conducted at the Beaufort Research/HMRC. The floating power device is a necessary unit in the wave energy converter (WEC) system. The dimensions and geometry of the FPS are similar to point absorber type WEC (which is believed to be the most typical WEC form). Damping corrections based on system identification effectively reduce the motion errors between the simulated time histories from SIMDYN and the measured time histories from the model tests. The system identification method is general enough, so it's expected to be applicable to many other wave energy structures (including WEC but not limited to other stuctures invloved in WEC systems, like the FPS in this study).

2. Reverse Multiple Input Single Output method

This section presents the Reverse Multiple Input Single Output (R-MISO), which is used to extract the transfer function and perform the coherence analysis. This section follows the complete derivation in [31].

Fig. 1a shows a multiple input single output (MISO) system, which consists of q inputs $x_i(t),\ i = 1, 2, \ldots, q$ and one output $y(t)$. System identification identifies the optimal transfer function from x_i to y, $H_{iy}(\omega)$, such that the noise $n(t)$ is minimized. The original inputs $x_i(t)$ can be converted into uncorrelated signals (in Fig. 1b) by conditioning an input with the previous inputs:

$$x_i(t) = x_{i:(i-1)!}(t) + x_{i.(i-1)!}(t) \tag{1}$$

$x_{i:(i-1)!}(t)$ is the part of x_i correlated with $x_1, x_2, \ldots, x_{i-1}(t)$ and $x_{i.(i-1)!}$ is the part uncorrelated with $x_1, x_2, \ldots, x_{i-1}(t)$. $L_{ij}(\omega)$ is the transfer function. Therefore, by taking Fourier transform of inputs, output and noise, the system can be expressed in the frequency domain as:

$$Y(\omega) = \sum_{i=1}^{q} L_{iy}(\omega) X_{i.(i-1)!}(\omega) + N(\omega) \tag{2}$$

Multiply both sides by $\frac{2}{T} X^*_{j.(j-1)!}$ and get the expected value while $T \to \infty$. In equation (3), "*" denotes the complex conjugate and "E" denotes the expected value.

$$\lim_{T\to\infty} \frac{2}{T} E\left[X^*_{j.(j-1)!} Y\right] = \lim_{T\to\infty} \frac{2}{T} \sum_{i=1}^{q} L_{iy} E\left[X^*_{j.(j-1)!} X_{i.(i-1)!}\right] + \lim_{T\to\infty} \frac{2}{T} E\left[X^*_{j.(j-1)!} N\right] \tag{3}$$

Each of the inputs $X_{i.(i-1)!}(\omega)$ and noise $N(\omega)$ are uncorrelated (zero cross spectra), and the conditioned inputs are uncorrelated internally (zero cross spectra). So the following equation is achieved:

$$S_{jy.(j-1)} = L_{jy} S_{jj.(j-1)!} \tag{4}$$

$S_{jy.(j-1)}$ is the conditional cross spectrum density and $S_{jy.(j-1)}$ is the conditional auto spectrum density. Similar to (4), the transfer functions $L_{rj}(\omega)$ between the conditioned inputs $x_{i.(i-1)!}(t)$ and one output $y(t)$ are given by:

$$S_{rj.(r-1)!} = L_{rj} S_{rr.(r-1)!} \tag{5}$$

More generally for $X_j(\omega)$, if $X_{j.r!}(\omega)$ represents the part of $X_j(\omega)$ that is uncorrelated with $X_1, X_2, \ldots, X_j$, then:

$$X_j(\omega) = \sum_{i=1}^{r} L_{ij}(\omega) X_{i.(i-1)!}(\omega) + X_{j.r!}(\omega) = \sum_{i=1}^{r-1} L_{ij}(\omega) X_{i.(i-1)!}(\omega) + X_{j.(r-1)!}(\omega) \tag{6}$$

Taking the difference between the two right hand sides of the

equations (6):

$$X_{j.r!}(\omega) = X_{j.(r-1)!}(\omega) - L_{rj}X_{r.(r-1)!} \tag{7}$$

Multiply both sides by $\frac{2}{T}X^*_{i.r!}$ and get the expected value under the limit $T \to \infty$:

$$S_{ij.r!} = S_{ij.(r-1)!} - \frac{S_{rj.(r-1)!}}{S_{rr.(r-1)!}} S_{ir.(r-1)!} \tag{8}$$

This is the recursion relation that can be used to calculate the conditioned cross spectrum $S_{ij.r!}$.

2.1 Transfer function

For the original (unconditioned) MISO system in Fig. 1a, the frequency domain output $Y(\omega)$ is:

$$Y(\omega) = \sum_{i=1}^{q} H_{iy}(\omega)X_i(\omega) + N(\omega) \tag{9}$$

Multiply (9) by $\frac{2}{T}X^*_{j.(j-1)!}$ and take the expected value while $T \to \infty$:

$$\lim_{T\to\infty}\frac{2}{T}E\left[X^*_{j.(j-1)!}Y\right] = \lim_{T\to\infty}\frac{2}{T}\sum_{i=1}^{q} H_{iy}E\left[X^*_{j.(j-1)!}X_i\right] + \lim_{T\to\infty}\frac{2}{T}E\left[X^*_{j.(j-1)!}N\right] \tag{10}$$

$$S_{jy.(j-1)!} = \sum_{i=j}^{q} H_{iy}\, S_{ji.(j-1)!} \tag{11}$$

Divide both sides by $S_{jj.(j-1)!}$ and substitute using (4) and (5):

$$L_{iy} = \sum_{i=j}^{q} H_{iy}\, L_{ji} \qquad i = 1, 2, \ldots, q \tag{12}$$

Equation (12) can be used to calculate H_{jy} from L_{jy} by subtracting backwards:

$$\begin{cases} H_{qy} = L_{qy} \\ H_{jy} = L_{jy} - \sum_{i=j+1}^{q} L_{ji}\, H_{iy} \qquad j = q-1, q-2, \ldots, 2, 1. \end{cases} \tag{13}$$

2.2 Partial coherence function

With the conditioning approach, the partial coherence functions, denoted as $\gamma^2_{iy.(i-1)}$, reveal the contribution of the conditioned inputs $x_{i.i-1}(t)$ to the output $y(t)$:

$$\gamma^2_{iy.(i-1)}(\omega) = \frac{|S_{iy.(i-1)}(\omega)|^2}{S_{ii.(i-1)}(\omega)S_{yy}(\omega)} \tag{14}$$

The sum of the first n ($n \le q$) partial coherence functions is the cumulative coherence function. The contribution from all the (q) inputs to the cumulative coherence function should always be less than equal to 1.

3. Model Test and Time Domain Analysis

The model tests of the floating power device (see Fig. 2) were performed at Beaufort Research/HMRC, Ireland [14]. The floating power device is a necessary unit in the wave energy conversion (WEC) system. It was selected because:

(1) Fully public model test data of wave energy devices is rare and very valuable. The data we used is open access and the necessary information for simulation is complete.

(2) The system identification method is general enough. Actually, the dimensions and geometry of the device are similar to a point absorber type wave energy converter (which is believed to be the most typical form).

An additional advantage makes the selected model tests more attractive:

(3) Many other open model test data of wave energy device measured the information of generated electricity (voltage, current) but the motion and time history (that we need the most) is not accessible. This study intentionally selected some tests in the rest/survival mode (when no power take off is in place) as it reduces uncertainties (the power take off is another nonlinear damping/dissipation, which is difficult to be simulated accurately without more details).

The incident wave headings are 0-degree, 30-degree and 60-degree. The 0-degree heading tests consists of much more sea states (wave) so the 0-degree wave heading series are selected for verification of SIMDYN and R-MISO analysis. The model test configuration is shown in Fig. 3 and as we can see the three mooring legs have azimuth difference between each other. The configuration (FPS geometry and mooring system configuration) is symmetric about the x axis, so we should expect relatively small motions in the sway, roll and yaw degree of freedom.

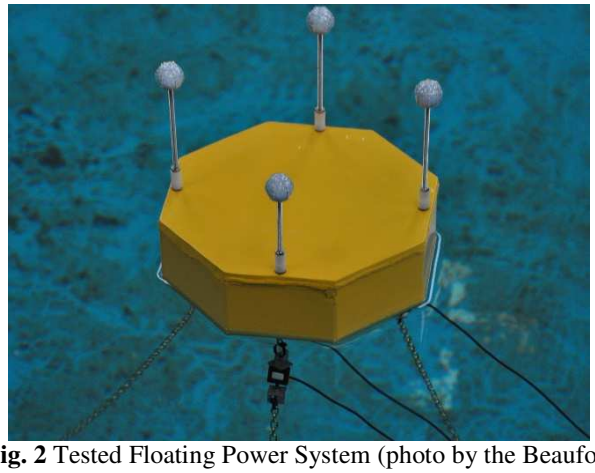

Fig. 2 Tested Floating Power System (photo by the Beaufort Research/HMRC, with permission)

From the 1:25 scale model tests, the calibrated incident wave at the FPS positions, the motions of the FPS in six degrees of

freedom, and the mooring line tensions at the three fairlead locations were measured and pre-processed by Beaufort Research/HMRC [14]. Wave was measured using two wire resistive type wave probes. The motion time series were output by the Qualisys track manager software. The mooring line forces were measured using Futek load cells.

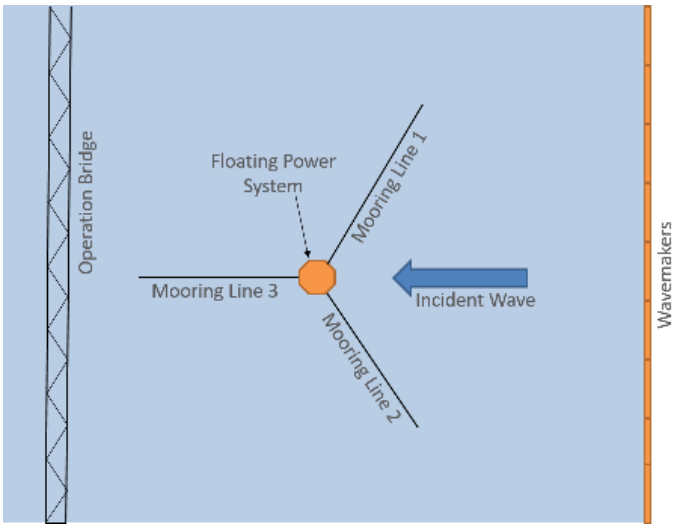

Fig. 3 0° wave test (experiments by Beaufort Research/HMRC, reproduced with permission)

The 0-degree wave heading tests consisted of 43 regular incident wave tests with wave height ranging from 1.0 m ~ 3.0 m and wave period ranging from 4.0 s ~ 17.5 s. The response amplitude operators from the model tests are plotted in Fig. 3 below.

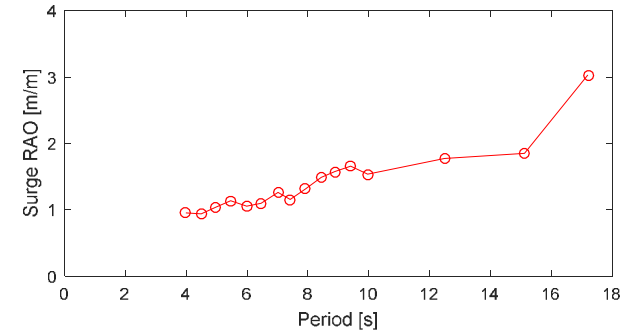

(a) Surge RAO

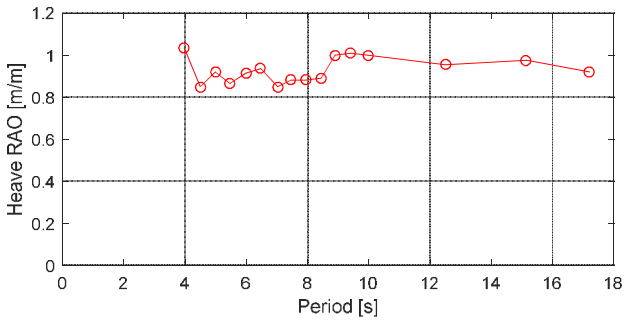

(b) Heave RAO

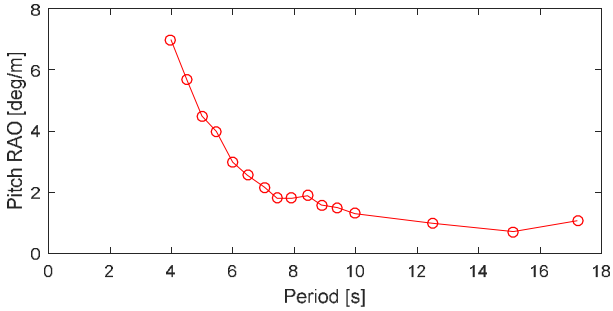

(c) Pitch RAO

Fig. 3 Response amplitude operators from model tests

For the three dominant motions: surge, heave and pitch, the average error between SIMDYN and the model tests is 5.8%, 4.3% and 6.4% respectively. The simulation errors are defined as follows:

$$Error = (std_{sim} - std_{exp})/std_{exp} \times 100\% \qquad (15)$$

std_{sim} and std_{exp} are the standard deviations from the simulations and experiments, respectively. Considering these errors are before any damping correction are made in the simulations, it means that SIMDYN yields relatively good accuracy in predicting the motions (at least for regular incident waves).

There are 20 irregular (random wave) cases in the 0-degree heading configuration, but some cases are ignored for the R-MISO analysis. The reasons for ignoring include that they may be not complete, or that the roll, yaw records are unexpectedly large (which should not be the case since the configuration is symmetric about the x-axis). Therefore, 12 cases are selected for system identification analysis and their spectra (Bretschneider) are shown in Fig. 4. Detail model test correlation will be demonstrated in the next section.

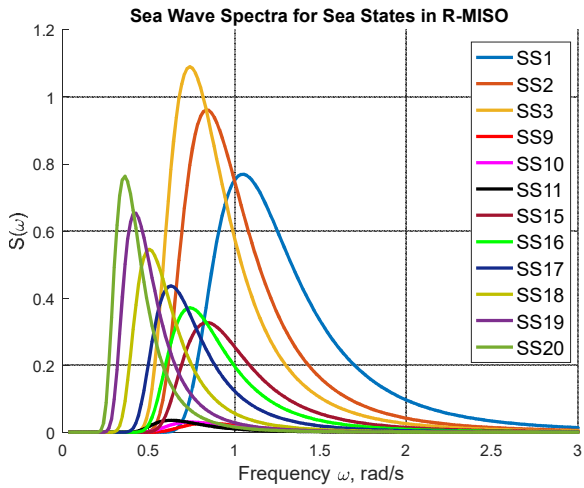

Fig. 4 Irregular sea states selected from R-MISO analysis

The time domain simulation is conducted with the in-house program SIMDYN [6] using the linear option for the inertia

forces, the Froude Krylov forces and the hydrostatic forces (as SIMDYN is an advanced blended time domain simulator and has a nonlinear option for those forces noted). The governing equation (see [32]) is:

$$[M + MA(\infty)]\ddot{x}(t) + Kx(t) + \int_0^t h(t-\tau)\ddot{x}(\tau) = F_e(t) \quad (15)$$

M is the mass matrix, $MA(\infty)$ is the added mass matrix at infinite frequency;

K is the hydrostatic stiffness;

$h(t-\tau)$ is the acceleration convolution integral function;

$F_e(t)$ are the total external forces. $F_e(t)$ includes the Froude Krylov forces, scattering forces, mooring forces, slowly varying wave drift forces, and drag forces (quadratic). Additional details concerning SIMDYN are published in [4].

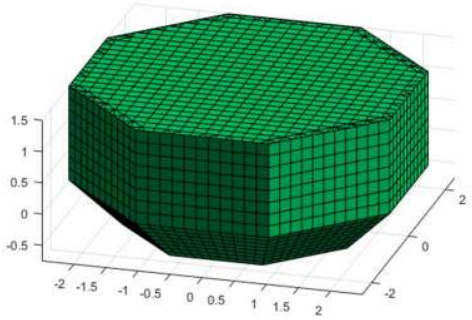

Fig. 5 Panel model of the FPS used in MDL-HYDROD

The Froude Krylov forces and scattering forces are obtained from the in-house frequency domain hydrodynamics analysis program MDL-HYDROD (refer to [11], [12] and [33]) and are converted from the frequency domain to the time domain in SIMDYN. Fig. 5 shows the panel model used in MDL-HYDROD. The origin (0, 0, 0) to define six degrees of freedom body motion is located on the calm water elevation of the central axis. The 3-leg mooring system is modeled by coupling SIMDYN (our in-house time domain simulator, FORTRAN) with the open-source Mooring Analysis Program (MAP++). MAP++ [9] is a library designed to model the Multi-Segmented, Quasi-Static (MSQS) mooring lines. MAP++ ignores the inertia forces of the mooring lines and the fluid drag forces on the mooring lines. Fig. 6 shows how MAP++ works with SIMDYN.

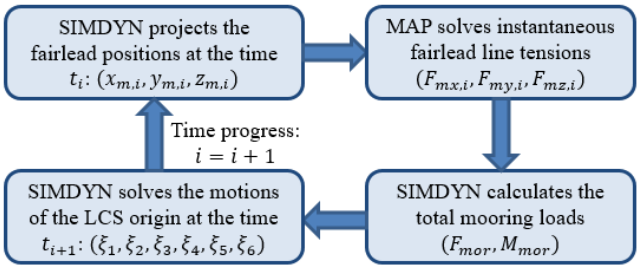

Fig. 6 Coupling of SIMDYN and MAP++

$(F_{mx,i}, F_{my,i}, F_{mz,i})$ denotes the instantaneous fairlead translation forces of mooring line number i. The fairlead position of mooring line number i, $x_{m,i} = (x_{m,i}, y_{m,i}, z_{m,i})$ is projected from the origin of the body coordinate system. The model test used the following parameters (1:25 scale) in the mooring modeling. The simulations and the experiments used the same mooring parameters to be as accurate as possible. Table 1 lists the important modeling parameters.

Table 1 Parameters for the floating power system

Particulars	Value
Mass *M* (kg)	11337.9
Length *Lpp* (m)	5.00
Breadth B (m)	5.00
Height *D* (m)	2.25
VCG (m)	0.64
Kxx (m)	1.386
Kyy (m)	1.386
Kzz (m)	1.821
Draft *T* (m)	0.75
Water Depth *h* (m)	25.0
Mooring Length (m)	75.0
Mass/Unit length (kg/m)	28.438
EA (N)	1.0×10^8
Scale of the Experimental Model	1:25

VCG is the vertical center of gravity and it is measured from the calm water plane (instead of from the bottom or keel of the body). *Kxx*, *Kyy* and *Kzz* are the gyradii, taken around the center of gravity. The motion responses (surge, heave and pitch) are compared in Table 2. The comparison of the motion responses is given by the ratio of the standard deviations from SIMDYN to those from the model tests.

Table 2 Motion responses ratio (SIMDYN/model test)

Sea state	Hs	Tp	Surge	Heave	Pitch
1	3.00	6.0	65.0%	101.2%	136.0%
2	3.00	7.5	67.9%	102.1%	133.0%
3	3.00	8.5	71.6%	102.4%	130.1%
9	0.50	7.5	92.8%	100.0%	96.4%
10	0.50	8.5	93.5%	100.5%	96.2%
11	0.50	10.0	92.7%	100.5%	95.9%
15	1.75	7.5	74.6%	100.2%	110.9%
16	1.75	8.5	81.4%	100.4%	108.1%
17	1.75	10.0	87.5%	100.6%	104.1%

18	1.75	12.5	89.9%	101.0%	107.4%
19	1.75	15.0	82.4%	101.2%	109.4%
20	1.75	17.5	81.0%	101.4%	110.6%
Average			81.7%	101.0%	111.5%

4. R-MISO Coherence Analysis

From the standard derivation comparison, we can find that the surge motion is about 18% lower than the model tests, this may be due to the inevitable discrepancy in modeling the mooring system. Inputs for the mooring system is estimated in this model test and that the surge motion is relative more sensitive to the mooring modeling.

The slowly varying wave drift forces may also account for part of the discrepancy. Even though the slowly varying wave drift forces are calculated from the full quadratic transfer function (QTF) matrix using Pinkster's approximation (see [10]) recently implemented in MDL's MDL-HYDROD (see [11]), the drift forces remain to be examined further.

Considering the uncertainties in the drift forces and mooring system modeling that significantly affects the surge motion more than the heave and the pitch, the surge motion will be studied but no damping or viscous drag correction will be implemented.

In addition, since it can be observed that case 1~3, case 9~11, case 15~17 and case 18~20 are similar in significant wave heights and standard deviations, they are put into 4 groups. The paper presents the analysis results of only the most representative cases selected from those groups for clearness.

The coherence analysis aims to reveal the most relevant input variables for a degree of freedom. If the partial coherence function for an input variable is not significant (always smaller than 0.1 or greater than 0.1 in frequency range where the motion power spectrum density, PSD, is very small), it means that the contribution from that input variable may be removed from the R-MISO analysis. In this way, the partial coherence functions can help us determine which input variables are suitable for R-MISO. In actual practice, it seems that sometimes R-SISO is good enough (e.g. for the heave) in getting good correlation between simulations and model tests.

In addition, the cumulative coherence functions are plotted to show the goodness for coherence analysis (presenting how much percentage of the output variable is contributed by the selected input variables). The motion power spectrum density (PSD) from the model tests is also plotted for the investigated degree of freedom. This is very helpful because we would not pay too much attention to the frequency range with little energy distribution (e.g. for pitch, frequency greater than 2.2 rad/s).

From the mass matrix in calculating the motion RAO, we know that the surge and the pitch is coupled (through the non-zero vertical center of gravity) while the heave is relatively independent. Consequently, for surge: the input variables are surge motion x_1, quadratic surge velocity v_1^2 and pitch motion x_5 while the output variable is surge diffraction (incident and scattering) excitation force (note that the drift force is not included in the R-MISO). Similarly, for the heave: the input variables are heave motion x_3 and quadratic heave velocity v_3^2 while the output variable is the heave diffraction (incident and scattering) excitation force. For pitch: the input variables are pitch motion x_5, quadratic pitch velocity v_5^2 and surge motion x_1 while the output variable is the pitch diffraction (incident and scattering) excitation moment.

4.1 Coherence function for the surge motion

Fig. 6 and Fig. 7 show the coherence analysis for the surge under sea state 3 and sea state 18, respectively. They are quite representative of the coherence functions for surge.

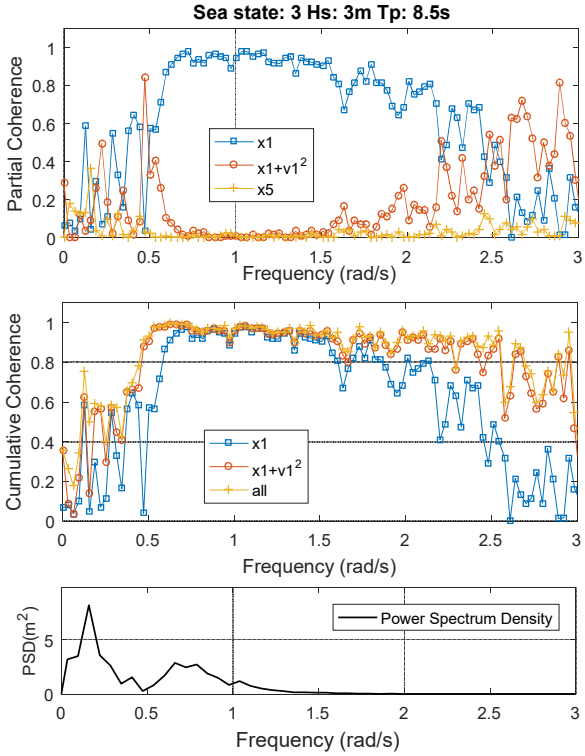

Fig. 6 Surge coherence analysis for sea state 3

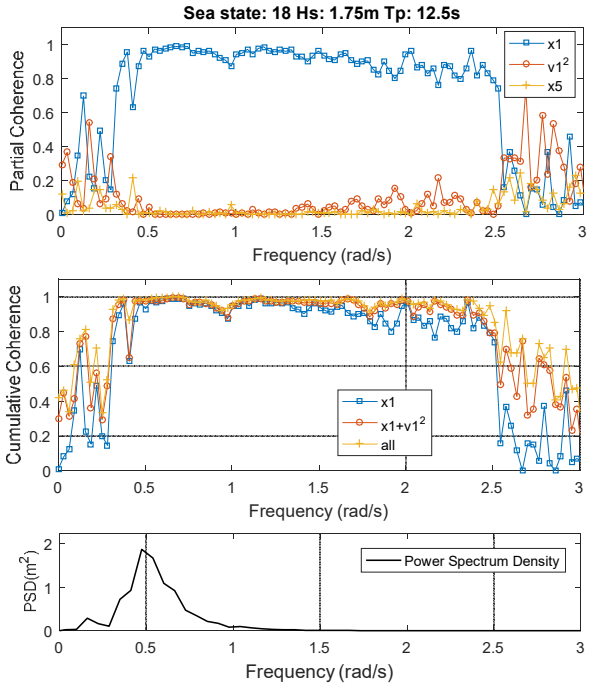

Fig. 7 Surge coherence analysis for sea state 18

We can find that the first input variable surge motion x_1 contributes above 80% while the quadratic surge velocity v_1^2 and pitch motion x_5 are usually small within important surge PSD range. We need to note that surge under sea state 3 is different from that under sea state 18 in that it has significant low frequency (largely drift contribution) but due to surge drift force assessment in SIMDYN and MDL-HYDROD, that part may not be captured well by the R-MISO technique at this moment. The R-SISO technique (the only input variable is the surge motion x_1) is therefore adopted for surge to help understand the linear damping in surge.

4.2 Coherence function for the heave motion

Fig. 8 and Fig. 9 show coherence analysis for the heave in sea state 3 and sea state 11, respectively. They are quite representative of the coherence functions for the heave.

We can find that the first input variable heave motion x_3 contributes above 95% (dominating) while the quadratic heave velocity v_3^2 contribution is small within important heave PSD range for the heave (0.4 rad/s ~ 1.6 rad/s). So the transfer function analysis of the heave is performed using the R-SISO technique and the only input variable is the heave motion x_3.

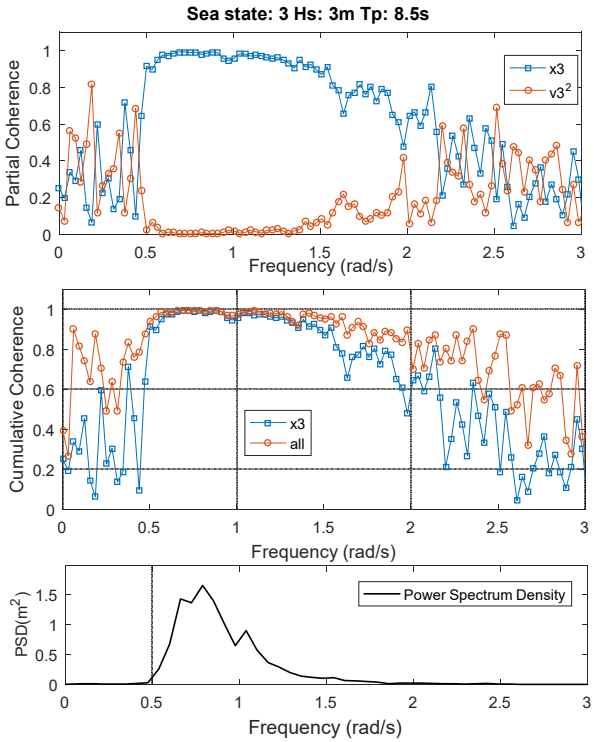

Fig. 8 Heave coherence analysis for sea state 3

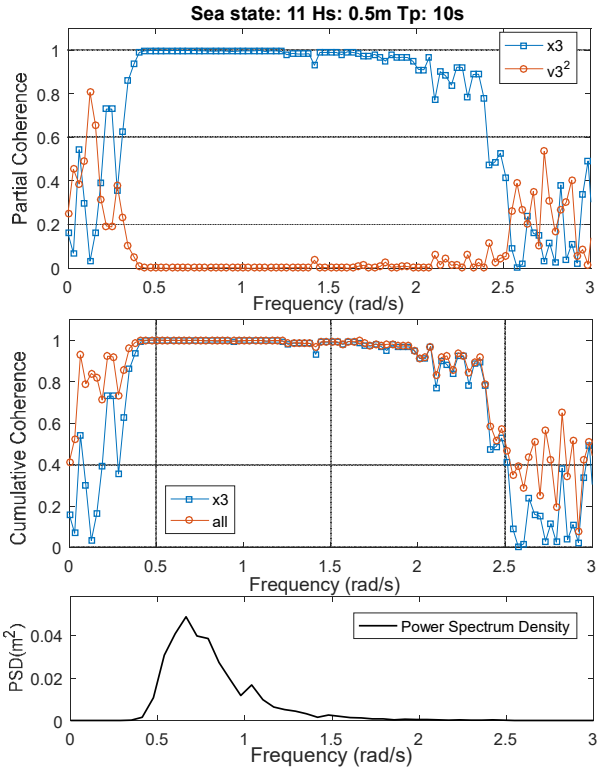

Fig. 9 Heave coherence analysis for sea state 11

4.3 Coherence function for the pitch motion

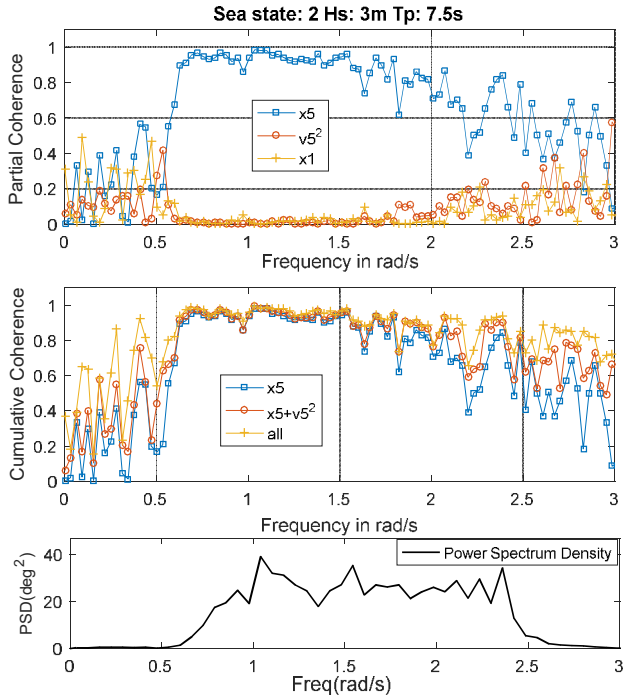

Fig. 10 Pitch coherence analysis for sea state 2

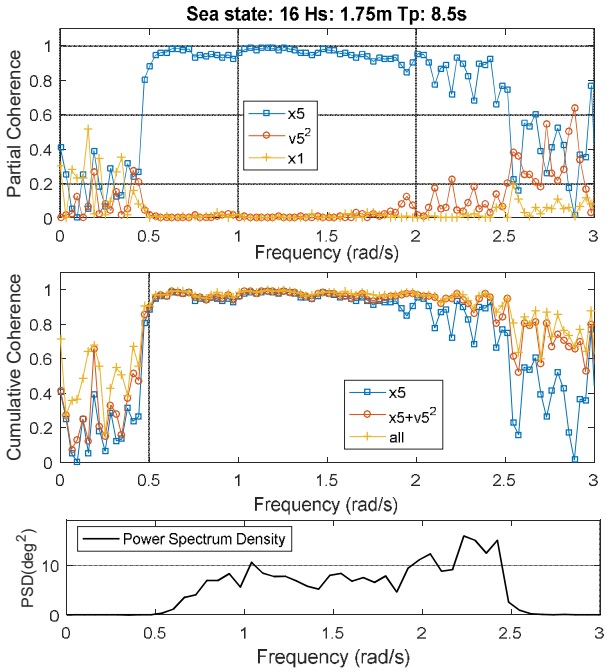

Fig. 11 Pitch coherence analysis for sea state 16

Fig. 10 and Fig. 11 show coherence analysis for the pitch in sea state 2 and sea state 16, respectively. They are quite representative of the coherence functions for pitch.

We can find that the first input variable pitch motion x_5 contributes above 60% and contribution from the quadratic pitch velocity v_5^2 is not negligible within important pitch PSD range (0.5 rad/s ~ 2.5 rad/s). The surge motion x_1 should also be included in R-MISO transfer function analysis after the surge motion (i.e. surge drift) can be modeled better. In the current R-MISO transfer function analysis for the pitch, the first input is the pitch motion x_5 and the other input is the quadratic pitch velocity $v_5|v_5|$.

5. R-MISO transfer function analysis

The generic transfer function from the motion x_i to the diffraction excitation F_i is:

$$H_{ii}(\omega) = K_{ii} - \omega^2[M + MA_{ii}(\omega)] + i\omega[D(\omega) + D_a(\omega)] \quad (16)$$

Besides the terms that have been declared in the equation (15), $D(\omega)$ is the (linear) radiation damping, which corresponds to energy dissipation in the radiated waves (excited by the oscillation of the structure).

$D_a(\omega)$ is the additional linear damping due to viscosity. The addition linear damping (and the additional quadratic damping) needs to be implemented because our (time domain) simulations is based on the potential flow theory. In the potential flow theory, viscosity of the fluid is not taken into consideration. $D_a(\omega)$ can be evaluated by several different methods (including free decay tests, system identifications). If no linear damping correction is made, $D_a(\omega)$ will be zero, which neglects the (linear) viscous effects.

Before an oscillatory flow separates from the surface of the body, the viscous damping force can be modeled well as a linear function of velocity. After an oscillatory flow separates from the surface of the body, the viscous damping force can be modeled more reasonably as a quadratic function of velocity.

The quadratic damping is also induced by viscosity. While the linear viscous damping is mainly attributed to the frictional force between the fluid and the submerged body (within the boundary layer), the quadratic damping is mainly induced by the flow separation as well as the vortex shedding. Actually, the two forms of the viscous damping are usually used together to better approximate the real viscous effects.

5.1 Transfer function for the surge motion

As discussed in section 4.1, R-SISO analysis is applied to the surge equation of motion. The surge transfer function shown in Fig. 12 is typical for the 12 irregular sea states. In the R-SISO analysis, the input is the surge motion time series (from the experiments and from the SIMDYN simulations, respectively) while the output is the surge force time series. The derived system identification technique in section 2.1 is used to calculate the transfer function from the time series.

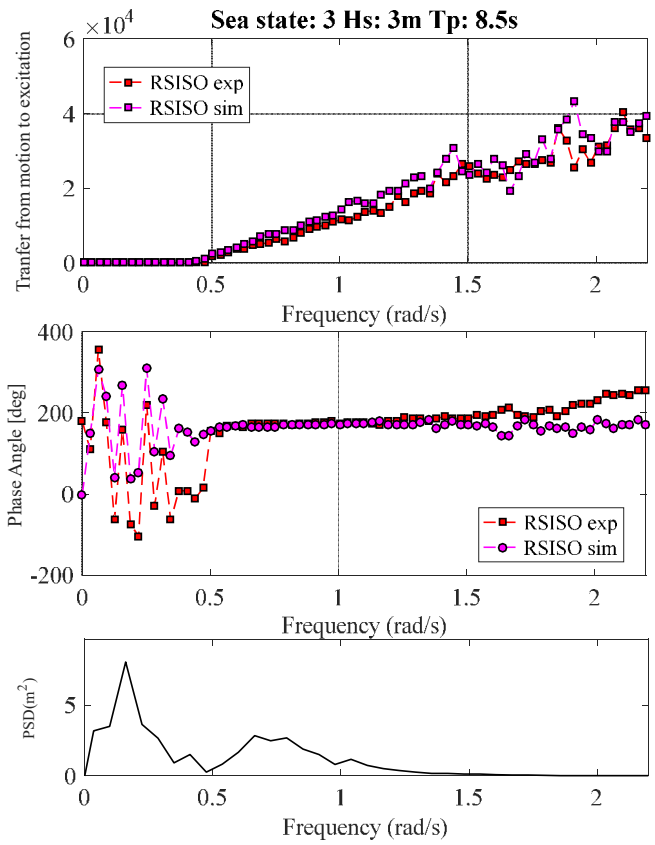

Fig. 12 Typical surge R-SISO results

In general, the transfer function for the wave frequency is modeled correctly. As much of the surge variance exists in the low frequency region that is closely related to the slowly varying surge drift force, modeling remains to be improved by better evaluation for the drift force.

5.2 Transfer function for the heave motion

As discussed in section 3.1, R-SISO analysis is applied to the heave motion. Fig. 13 and Fig. 14 show the typical heave transfer functions. In general, from R-SISO analysis, we can tell that the heave motion is modeled very accurately even before any damping correction is made.

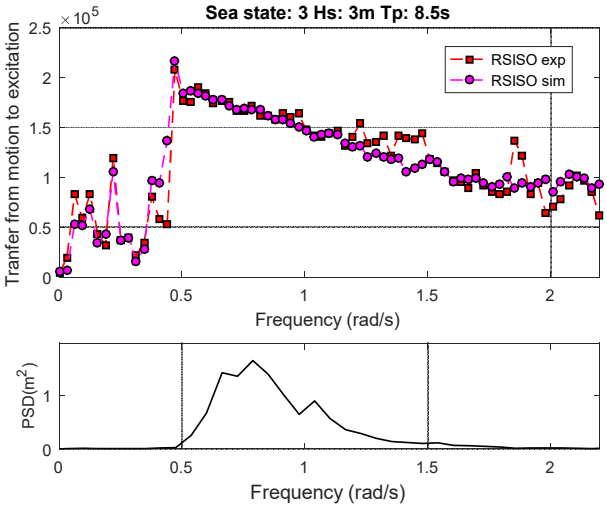

Fig. 13 Sea state 3 heave transfer function from R-SISO

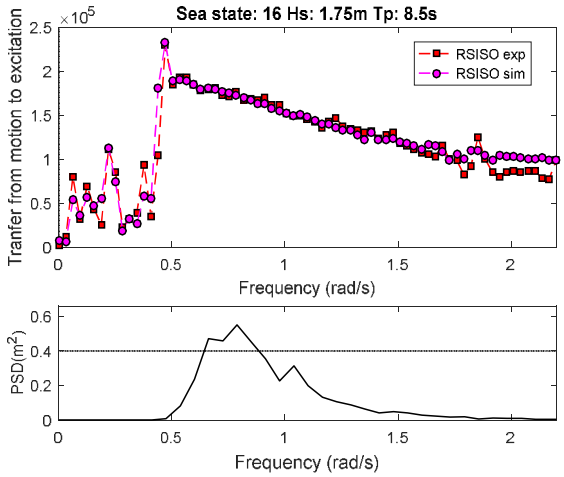

Fig. 14 Sea state 16 heave transfer function from the R-SISO

In addition, when Fig. 13 and Fig. 14 is compared, it can be found that the R-SISO technique works better with the milder sea state. Heave motion can be modeled quite well with the generic transfer function (16) but as the sea state (wave height) increases, the accuracy of the equation (16) decreases.

Considering that the heave standard deviation difference between the model tests and the SIMDYN results are already within 2.5% (on an average 1.0% error only), it's believed that additional damping correction is not necessary.

Fig. 15 is a typical heave time series comparison with the model test. The simulation program directly takes the calibrated wave time history at the FPS's moored position (provided by the Beaufort Research/HMRC, Ireland) for the corresponding sea states. The calibrated waves are repeatable. Therefore, when the FPS is in place, the incident wave is identical to the calibrated wave. This confirms that for the heave the R-SISO method is good enough.

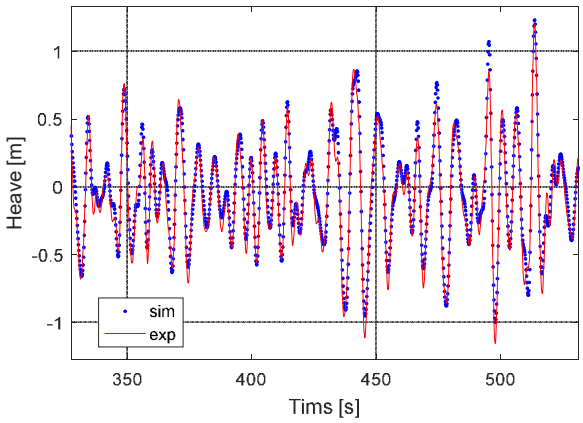

Fig. 15 Sea state 16 heave correlation with model test

5.3 Transfer function for the pitch motion

The R-MISO technique becomes most valuable for the study of the pitch motion. The first transfer function between the pitch motion and the pitch moment is the equation (16) while the second transfer function H_q satisfies the equation (17) below ([32] & [34]):

$$H_q \cdot (v_i|v_i|) = F_q \tag{17}$$

F_q is the quadratic damping force. H_q, the second transfer function is usually determined from the model test. Remind the typical formula for the drag force:

$$\frac{1}{2}\rho C_D A \cdot (v_i|v_i|) = F_q \tag{18}$$

By comparing equation (17) with equation (18), it is reasonable to assume that the second transfer function H_q (i.e. the quadratic damping) is a coefficient.

Using the R-MISO technique, we can assess how much linear damping in the equation (16) and quadratic damping in the equation (17) that needs to be added into the simulation. Based on the transfer function, we may make corrections to those damping in the time domain simulations.

Sea state 2 is a typical case that the linear damping needs to be compensated. The square of transfer function error is the indicator for deciding the damping corrections. The procedure is (take sea state 2 as an example):

(1) Estimate the range of damping correction [0, 5×10^4] (using the step of 1×10^4) and run the simulations with these damping corrections;

(2) Perform the system identification analysis to get the transfer functions from these simulations;

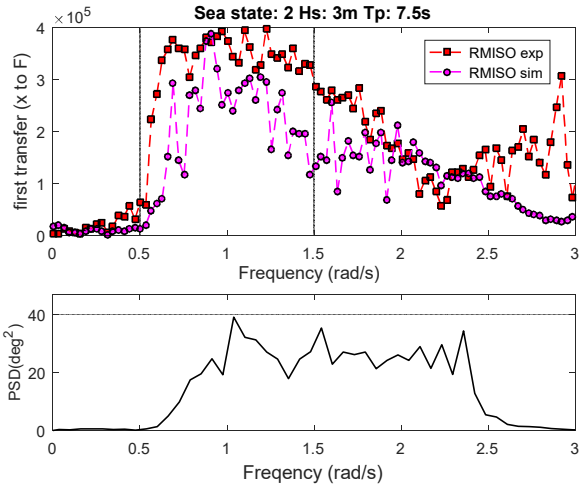

Fig. 16 Sea state 2 pitch transfer function from R-MISO

Fig. 16 shows the pitch transfer function from R-MISO. Please note that only the first transfer function (from the pitch motion to the pitch moment) is plotted because the second input (quadratic pitch velocity) is conditioned using the first input, therefore, it's always important to correct the first transfer function first.

(3) Get the error indicator Se (sum of the transfer function errors' squared):

$$Se = \sum_{i=1}^{NF}\left[|H_{sim}(\omega_i)| - |H_{exp}(\omega_i)|\right]^2 \tag{18}$$

(4) Plot Se to select the damping correction that best fit the transfer function in the simulation to the transfer function in the model test:

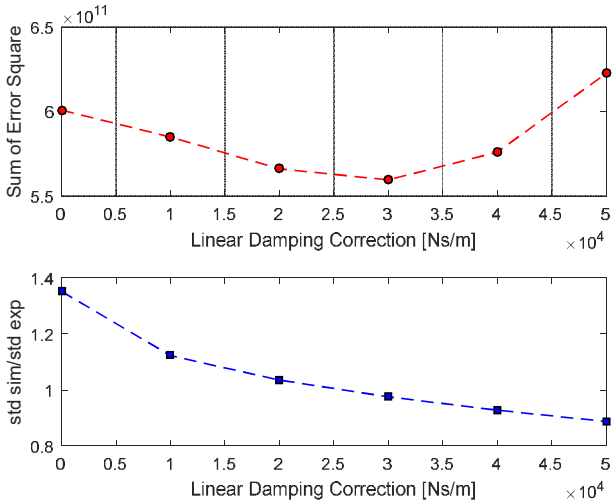

Fig. 16 Determining sea state 2 linear damping

(5) Damping correction $3\times10^4\ N\cdot m/(rad/s)$ makes the best transfer function fitting, so $3\times10^4\ N\cdot m/(rad/s)$is the linear damping we propose. (We can tell from the standard deviation

comparison that this is a good value.)

Using similar method, the quadratic damping corrections can also evaluated (see the next example, sea state 20). Based on Fig. 16 and the equation (16), additional $3\times10^4\ N\cdot m/(rad/s)$ linear damping is estimated and should be implemented into the time domain simulation. Fig. 17 shows the pitch transfer function from R-MISO after the damping correction. In general, the comparison improved over the frequency range 0.5 rad/s ~ 2.7 rad/s (from the pitch PSD).

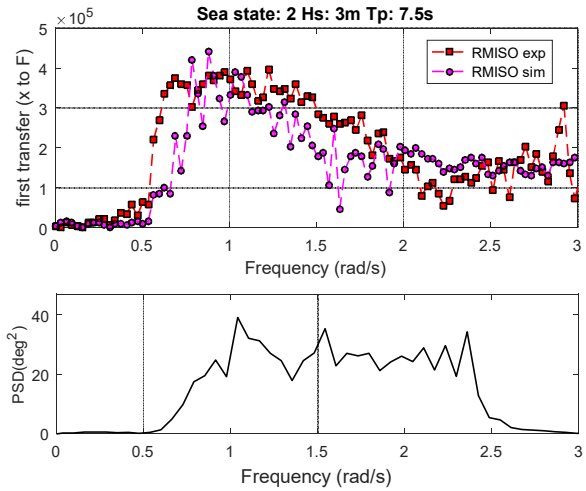

Fig. 17 Sea state 2 pitch (after linear damping correction) the transfer function from R-MISO

Correspondingly, in the time domain simulation, the standard deviation error drops significantly from 33.0% to -3.4%. The better correlation can also be observed in Fig. 18.

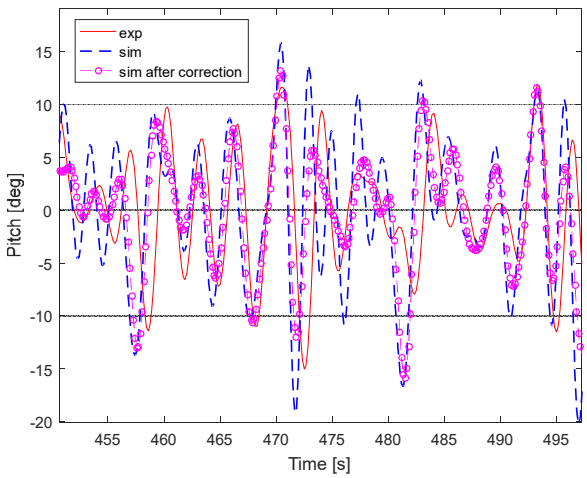

Fig. 18 Sea state 2 pitch time series comparison

It can be observed that the pitch motion comparison in Fig. 18 is not as perfect as the heave motion comparison in Fig. 15. For pitch, the test target is symmetric (meaning it is same with 90-degree rotation around z-axis). Therefore, the pitch motion is in this sense similar to roll motion (remind that roll damping for ship is notoriously complicated). The most common, linear time domain potential flow method is what we used in this study (SIMDYN). If we stick to this method, further improvements are very limited. However, we have implemented in SIMDYN the capability of using the blended time domain potential flow method (can better handle the instantaneous Froude-Krylov and hydrostatic forces). That will improve the time series comparison (at the cost of calculation time) [6].

Sea state 20 is a typical case that the quadratic damping needs to be compensated for. Fig. 19 shows the pitch transfer function from R-MISO. The first transfer function (from the pitch motion to the pitch moment) yields reasonable comparison with the model test while the second transfer function is low compared to the model test.

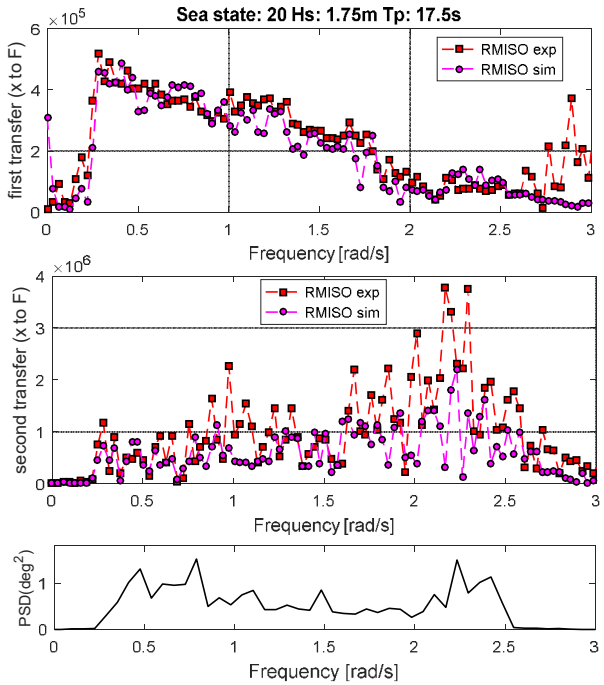

Fig. 19 Sea state 20 pitch transfer functions from R-MISO

Based on Fig. 19 and the equation (17), additional $2\times10^5\ N\cdot m/(rad/s)^2$ quadratic damping is estimated and is implemented into the time domain simulation. Fig. 20 shows the second transfer function (the corresponding input is the quadratic pitch velocity) from R-MISO after the damping correction. In general, the comparison improved over the frequency range 0.3 rad/s ~ 2.5 rad/s (from the pitch PSD).

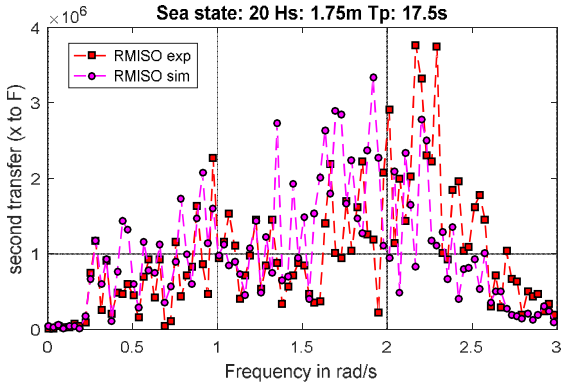

Fig. 20 Sea state 20 pitch transfer functions from R-MISO

Correspondingly, in the time domain simulation, the standard deviation error drops significantly from 10.6% to 2.0%. The improved model test correlation can also be observed in Fig. 21.

For pitch, since the test target is symmetric (meaning it is same with 90-degree rotation around z-axis), the pitch motion is similar to roll motion (remind that roll damping for ship is notoriously complicated). The time series comparison can be further improved by using higher fidelity modelling. In fact, we are extending SIMDYN's capability of using the blended time domain method (will better handle the instantaneous Froude-Krylov and hydrostatic forces). That will improve the time series comparison (at the cost of calculation time).

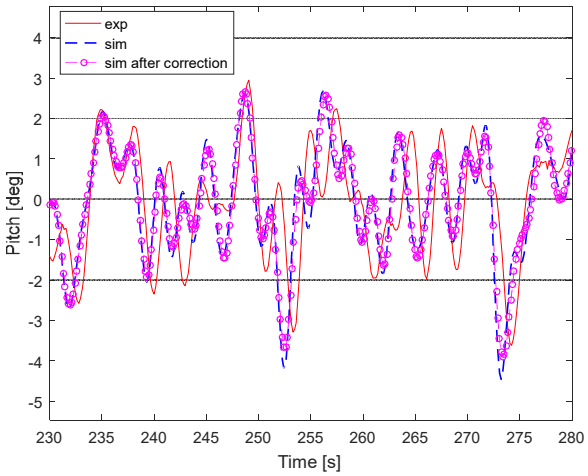

Fig. 21 Sea state 2 pitch time series comparison

Similar corrections are made for other irregular sea states. The damping corrections revealed by system identification and the standard deviation improvements are listed in Table 3. In general, the error of standard deviation is reduced from 11.5% to -1.9%.

Table 3 Motion responses ratio (SIMDYN/model test)

Sea state	Linear correction	Quadratic correction	Pitch w/o correction)	Pitch w. correction)
1		5.0×10^4	136.0%	100.1%
2	3.0×10^4		133.0%	96.6%
3	3.0×10^4		130.1%	96.0%
9			96.4%	96.4%
10			96.2%	96.2%
11			95.9%	95.9%
15		5.0×10^4	110.9%	97.0%
16		5.0×10^4	108.1%	98.3%
17		5.0×10^4	104.1%	97.4%
18		1.0×10^5	107.4%	100.8%
19		1.5×10^5	109.4%	100.5%
20		2.0×10^5	110.6%	102.0%
Average			111.5%	98.1%

5.4 Discussions of R-MISO transfer function analysis

Conventionally the viscous damping can be estimated by:

a) Empirical formula: give (rough) estimations of the damping but the accuracies vary significantly.

b) Free decay tests: only provide the damping at the natural frequency.

c) Forced oscillation tests: test facilities are very expensive. What's more, they are generally limited to model scale.

In the model tests of the floating power system (by Beaufort Research/HMRC), free decay tests or forced oscillation tests were not performed. There is no empirical formula appropriate for this geometry (as it is a relatively novel form of a floating wave energy device). System identification is not just the choice when other alternatives are absent, it (i.e. R-MISO in this paper) is superior to other methods a)-c) in that:

- It reveals the variation of quadratic (and linear) damping with frequency, which cannot be effectively done otherwise.
- It can directly deal with cases under random sea states, which is the most meaningful situations, as the actual sea state is random.

Using Reverse-MISO, not only a constant additional quadratic damping at the natural frequency can be obtained such as using a free decay test (no incident wave involved) but that the frequency dependent effective ("effective" means that incident waves are present , and it is therefore more realistic) damping can be obtained. In fact, the viscous damping itself under different sea states varies considerably (in this study, the wave height ranges from 0.5 m to 3.75 m and peak period ranges from 6.0 s to 17.5 s). The fact that system identification provides the frequency dependent damping instead of a constant damping is

an significant advantage in reducing the simulation errors. In fact, using system identification has improved considerably the accuracy of motion predictions compared to using empirical formula or free decay test results as was done in many other studies (see [4], [16] and [30]). If the viscous damping is taken as a constant (from the free decay test), then the overall simulation errors (for all the sea states) will remain at a higher level.

6. Conclusions

The paper presents the first application of the R-MISO system identification technique to the model test correlation for a wave energy device (the floating power system). The technique is primarily applied to validate the time domain simulation model and screen for critical input variables for motion in a degree of freedom. That practically helps us better interpret the time domain results. In naval architecture and ocean engineering research, previous studies have seen applications of the system identification method to a moving ship. This paper applies the method to a stationary (i.e., realistically moored) non-ship-shape geometry.

Coherence analysis through system identification provides a frequency domain perspective to examine the simulation of a wave energy device. For this wave energy device, coherence analysis reveals that the heave degree of freedom can be modeled well even without damping corrections as a single input (heave motion) single output (heave force) system. Both linear damping and quadratic damping contribute considerably to the pitch motion in the multiple inputs (pitch motion and quadratic pitch velocity) single output (pitch moment) system. Coherence analysis shows that the surge motion is more sensitive to the low frequency drift forces. Further improvements of the simulation program are needed to better carry out the R-MISO analysis on the surge motion.

Furthermore, the transfer function analysis is performed to assess the necessary damping corrections under the irregular sea states based on the model tests data. Implementing the damping correction revealed from the system identification method effectively improves the accuracy of the time domain simulations and should be a valuable correction to the time domain simulation of the wave energy devices.

This study, for the first time, applied the reverse-MISO to a realistically (catenary) moored system, which represents typical characteristics of wave energy devices. Compared to previous studies, the increased complexity of our modelling (6 or 3 degrees of freedom with catenary mooring modelling) is definitely progress in application of the R-MISO system identification as an advanced analysis methodology. Our research shows that R-MISO can be applied to model test correlations of moored floating structures, which categorize the majority of wave energy devices and floating offshore platforms.

Acknowledgements

The authors would like to acknowledge the Beaufort Research/HMRC and Dr. Bret Bosma for providing the complete model test data and detail information. The open source mooring code MAP++ developed by Dr. Marco Masciola is a necessary and efficient component in performing the time domain simulations successfully. Discussions with Dr. Jason Jonkman and Dr. Yi-Hsiang Yu from National Renewable Energy Laboratory have also been very helpful for this work.

REFERENCES

[1] A.F.de.O. Falcão, Wave energy utilization: a review of the technologies, Renew. Sustain. Energy 14(3) (2010) 899-918.
[2] H. Wang, J.M. Falzarano, Energy balance analysis method in oscillating type wave converter, J. Ocean Eng. Mar. Energy 3(3) (2017) 193-208.
[3] B. Drew, A. Plummer, M. Sahinkaya, A review of wave energy converter technology, Proceedings of the Institution of Mechanical Engineers, Part A: Journal of Power and Energy 223 (2009) 887–902.
[4] A. Somayajula, Reliability Assessment of Hull Forms Susceptible to Parametric Roll in Irregular Seas (Ph.D. dissertation), Texas A&M University, College Station, 2017.
[5] A. Somayajula, J.M. Falzarano, Large-amplitude time-domain simulation tool for marine and offshore motion prediction, Mar. Syst. Ocean Technol. 10(1) (2015) 1–17.
[6] H. Wang, A. Somayajula, J.M. Falzarano, Z. Xie, Development of a blended time-domain program for predicting the motions of a wave energy structure. J. Mar. Sci. Eng. 8(1) (2020).
[7] A. Somayajula, J.M. Falzarano, Validation of Volterra series approach for modelling parametric rolling of ships, in: Proceedings of 34th International Conference on Ocean, Offshore and Arctic Engineering, St. John's, Canada, 2015.
[8] A. Somayajula, J.M. Falzarano, A comparative assessment of approximate methods to simulate second order roll motion of FPSOs. Ocean Systems Engineering, 7(1), (2017) 53–74.
[9] M. Masciola, MAP++ Documentation Release 1.15, https://map-plus-plus.readthedocs.io/en/latest (accessed 12 Feb 2018)
[10] J. Pinkster, Low Frequency Second Order Wave Exciting Forces on Floating Structures (Ph.D. dissertation), Delft University of Technology, Netherlands, 1980.
[11] Z. Xie, Y. Liu, J.M. Falzarano, A numerical evaluation of the quadratic transfer function for a floating structure, in: Proceedings of the ASME 2019 38th International Conference on Ocean, Offshore and Arctic Engineering, Glasgow, UK, 2019.
[12] A. Guha, Development of a Computer Program for Three Dimensional Frequency Domain Analysis of Zero Speed First Order Wave Body Interaction (Master's thesis), Texas A&M University, College Station, 2012.
[13] A. Elhanafi, G. Macfarlane, A. Fleming, Z. Leong, Experimental and numerical investigations on the intact and damage survivability of a floating-moored oscillating water column device, Appl. Ocean Res. 68 (2017) 276-292.
[14] B. Bosma, W. Sheng, F. Thiebaut, Performance assessment of a floating power system for the Galway Bay wave energy test site, in: International Conference on Ocean Energy, Halifax, Canada, 2014.
[15] T. Lettenmaier, E. Amon, A. Jouanne, Power converter and control system developed in the ocean sentinel instrumentation buoy for testing wave energy converters, in: IEEE Energy

Conversion Congress and Exposition (ECCE), Denver, USA, 2013.
[16] S. Sirnivas, Y.H. Yu, M. Hall, B. Bosma, Coupled mooring analyses for the WEC-SIM wave energy converter design tool, in: Proceedings of the ASME 2016 35th International Conference on Ocean, Offshore and Arctic Engineering, Busan, South Korea, 2016.
[17] J.M. Falzarano, A. Somayajula, R. Seah, An overview of the prediction methods for roll damping of ships, Ocean Syst. Eng. 5 (2) (2015) 55–76.
[18] A. Somayajula, J.M. Falzarano, Critical assessment of reverse-MISO techniques for system identification of coupled roll motion of ships, J. Mar. Sci. Technol. (2016) 1–19.
[19] S.F. Masri, R.K. Miller, A.F. Saud, T.K. Caughey, Identification of nonlinear vibrating structures: part I formulation, J. Appl. Mech. 54 (4) (1987) 918–922.
[20] S.F. Masri, R.K. Miller, A.F. Saud, T.K. Caughey, Identification of nonlinear vibrating structures: part II applications, J. Appl. Mech. 54 (4) (1987) 923–929.
[21] I.J. Leontaritis, S.A. Billings, Input–output parametric models for non-linear systems: part I. deterministic non-linear systems, Int. J. Control 41 (2) (1985) 303–328.
[22] I.J. Leontaritis, S.A. Billings, Input–output parametric models for non-linear systems: part II. Stochastic non-linear systems, Int. J. Control 41 (2) (1985) 329–344.
[23] M. Feldman, Non-linear system vibration analysis using Hilbert transform: part I free vibration analysis method 'Freevib', Mech. Syst. Signal Process. 8 (2) (1994) 119–127.
[24] M. Feldman, Non-linear system vibration analysis using Hilbert transform: part II Forced vibration analysis method 'Forcevib', Mech. Syst. Signal Process. 8 (3) (1994) 309–318.
[25] J. Bendat, A. Piersol, Random Data: Analysis and Measurement Procedures, 4th ed., John Wiley & Sons, New York, 2011.
[26] J.S. Bendat, P.A. Palo, Nonlinear System Stochastic Techniques for Ocean Engineering Applications, Tech. Rep., Naval Civil Engineering Laboratory, Port Hueneme, USA, 1989.
[27] J. Bendat, Nonlinear System Analysis and Identification from Random Data, 1st ed., John Wiley & Sons, New York, 1990.
[28] J. Falzarano, J. Cheng, W. Rodrigues, Transit draft heave and pitch motion analysis of the mobile offshore base (MOB) using reverse MI/SO techniques, J. Offshore Mech. Arct. Eng. 126 (1) (2004) 16-25.
[29] J. Cheng, J.M. Falzarano, System identification of nonlinear coupled ship/offshore platform dynamics in beam seas, in: Proceedings of ASME 2003 22nd International Conferences on Ocean, Offshore and Arctic Engineering, ASME, Cancun, Mexico, 2003, pp. 531–540, ISBN 0-7918-3681-9.
[30] A. Somayajula, J.M. Falzarano, Estimation of roll motion parameters using R-MISO system identification technique. In Proceedings of 26th International Offshore and Polar Engineering (ISOPE) Conference, Rhodes, Greece, 2016.
[31] A. Somayajula, J. M. Falzarano, Application of advanced system identification technique to extract roll damping from model tests in order to accurately predict roll motions, Appl. Ocean Res. 67 (2017) 125–135.
[32] ANSYS Inc., AQWA-DRFT User Manual, https://manualzz.com /doc/6968868/aqwa-drift-manual (accessed 1 Sep 2018)
[33] Y. Liu, J.M. Falzarano, Suppression of irregular frequency effect in hydrodynamic problems and free-surface singularity treatment, J. Offshore Mech. Arct. Eng. 139(5) (2017) 1-16.
[34] Orcina Ltd. UK, OrcaFlex Documentation, http://www.orcina.com /Software/Products/OrcaFlex/Documentation/Help (accessed 12 Feb 2019)